HAL open science

Hybrid Methods for Duct Aeroacoustics Simulations

Silouane De Reboul, Emmanuel Perrey-Debain, Stephane Moreau, Nicolas Zerbib

To cite this version:

Silouane De Reboul, Emmanuel Perrey-Debain, Stephane Moreau, Nicolas Zerbib. Hybrid Methods for Duct Aeroacoustics Simulations. Forum Acusticum, Dec 2020, Lyon, France. pp.387-391, 10.48465/fa.2020.0616 . hal-03221406

HAL Id: hal-03221406

https://hal.science/hal-03221406v1

Submitted on 20 May 2021

HAL is a multi-disciplinary open access archive for the deposit and dissemination of scientific research documents, whether they are published or not. The documents may come from teaching and research institutions in France or abroad, or from public or private research centers.

L'archive ouverte pluridisciplinaire **HAL**, est destinée au dépôt et à la diffusion de documents scientifiques de niveau recherche, publiés ou non, émanant des établissements d'enseignement et de recherche français ou étrangers, des laboratoires publics ou privés.

HYBRID METHODS FOR DUCT AEROACOUSTICS SIMULATIONS

Silouane de Reboul[123] **Emmanuel Perrey-Debain**[1] **Stéphane Moreau**[2]
Nicolas Zerbib[3]
[1] Université de Technologie de Compiègne, Compiègne, France
[2] Université de Sherbrooke, Sherbrooke, Canada
[3] ESI-Group, Toulouse, France
silouane.de-reboul@utc.fr

ABSTRACT

In this paper, several different aeroacoustic approaches are presented, combining Finite Element implementations of Lighthill's and Ribner's analogies with an estimation of the aerodynamic noise sources with Computational Fluid Dynamics. The source computation relies on Large Eddy Simulation with the software OpenFOAM. The source information is mapped on a coarser acoustic mesh to compute the acoustic propagation with a Finite Element solver working in the frequency domain. This procedure has been applied to predict the sound generated by a 3D ducted diaphragm. The result obtained are compared with experimental ones. Both numerical approaches are in a good agreement with the measurements. Lighthill's analogy seems to be slightly more accurate but is more complex to carry out: the source computation is not as trivial as Ribner's source, and the volume of the data needed is more significant. Both approaches seem therefore applicable for industrial applications.

1. INTRODUCTION

In the coming years, more hybrid and full electric vehicles will be coming to the market and some new challenges will arise for noise and vibration engineers. One of them is the flow-induced sound: the noise perceived by a car driver comes from many different sources, among which several belong to aerodynamics. At high speed, the noise of the turbulent wake generated by the side mirrors, the windshield wipers, etc. becomes dominant. There are also internal aerodynamic noise sources, such as the fan noise in the ventilation system, or in the engine or battery cooling devices. Furthermore, in electric cars the engine is way more silent when the vehicle is moving, and therefore other noise source become predominant, leading to a greater impact of aerodynamic noise [1].

Simulating aerodynamic noise is not an easy task since the classical approach in acoustics is to study small perturbation of an equilibrium state of a fluid at rest. In aeroacoustics, neither of these hypothesis are verified. A possible approach is to start from the same equations, the fluid dynamics equations, without linearizing them. Two kinds of approaches are possible. With the *direct methods*, these equations are fully resolved in order to allow the sound waves to exist in the simulation. This requires a high degree of accuracy since the acoustic and aerodynamic spacial and temporal scales are quite different. Opposed to the direct method, the *hybrid* ones allow us to reduce the CFD cost by decoupling the noise generation from its propagation. They rely on the assumption that the acoustic fluctuation do not alter the flow and are commonly used for low Mach number flows. The sound transport is generally based on *Aeroacoustic Analogies*, a reformulation of the fluid dynamics equations bringing out a wave equation and an aerodynamic source. This source can be estimated with analytical or semi-analytical models, or with CFD calculations. [2]

In an industrial context, the aim is to be able to predict aeroacoustics in complex geometries at an affordable cost. For these reasons, the methods considered in this paper are hybrid methods based on *Computational Fluid Dynamics* (CFD) to obtain the noise sources, and an *Finite Element Method* (FEM) computation based on acoustic analogies to propagate the sound.

Several analogies are compared and applied to a ducted air flow. First, theoretical models and different analogies are presented. Then, the test case and the experimental setup used to validate the results are described. The CFD computation to obtain the sources is then presented, as well as the steps of the procedure. Finally, results are compared and the applicability of the methods in an industrial context is discussed.

2. HYBRID APPROACH FOR AEROACOUSTICS

2.1 Aeroacoustic Analogies

Sir James Lighthill laid the foundations of aeroacoustics in 1952 by manipulating the Navier-Stokes equations to yield a wave equation. The divergence of the momentum conservation law subtracted from the temporal derivative of the mass conservation law leads to:

$$\left(\frac{1}{c_0^2}\frac{\partial^2}{\partial t^2} - \Delta\right) p' = \frac{\partial^2}{\partial x_i \partial x_j}(\rho u_i u_j - \tau_{ij}) + \frac{\partial^2}{\partial t^2}\left(\frac{p'}{c_0^2} - \rho'\right). \quad (1)$$

p' and ρ' are the fluctuations of the static pressure p_s and density ρ. u is the flow velocity and τ the tensor of viscous constraints. This equation (*Lighthill's analogy*) is obtained without linearization, no assumption is made about

the fluctuations of the pressure around its equilibrium, and this exact equation allows the sound to be generated from nonlinear flows [3].

Some hypothesis are required to simplify the source term and make this equation solvable: the viscosity is neglected for high Reynolds numbers, the flow is supposed isentropic, and at low Mach number it is considered as incompressible. Those hypothesis and the consideration of a harmonic acoustic pressure lead to the following Helmholtz equation:

$$\left(\Delta + k^2\right) p = -\frac{\partial^2}{\partial x_i \partial x_j}(T_{ij}), \tag{2}$$

where $T_{ij} = \rho_0 u_i u_j$ is the simplified Lighthill's tensor, k is the wavenumber $\frac{\omega}{c_0}$ and p is now the Fourier component of the pressure fluctuation. Ribner introduced another way of simplifying the source term: he separates the pressure fluctuations into a sum of a quasi incompressible component $p^{(0)}$ called *pseudo-sound*, and an "acoustic" pressure $p^{(1)}$ [4].

$$p = p^{(0)} + p^{(1)}. \tag{3}$$

$p^{(0)}$ is defined by $\Delta p^{(0)} = -\frac{\partial^2}{\partial x_i \partial x_j}(\rho_0 u_i u_j)$, and therefore it is possible to rewrite equation (2) as follows:

$$\left(\Delta + k^2\right) p^{(1)} = -k^2 p^{(0)}. \tag{4}$$

This relation is called the *dilatation equation*.

2.2 Resolution with the Finite Element Method

The *Finite Element Method* (FEM) is well suited for solving the previous equations. The idea of implementing an analogy with the Finite Element Method has been proposed by Oberai *et al.* [5] and further extended by Caro *et al.* [6]. The domain studied is called Ω and its boundary Γ as shown in Figure 1. The standard FEM variational formulation of equation (2) is the following, with ϕ a test function:

$$-\int_\Omega \nabla\phi\nabla p \, dV + k^2 \int_\Omega \phi p \, dV + \int_\Gamma \phi \partial_n p \, dS = \int_\Omega \nabla\phi \cdot (\underline{\underline{\nabla}} \cdot T_{ij}) \, dV - \int_\Gamma \phi \, (\underline{\underline{\nabla}} \cdot T_{ij}) \cdot n \, dV. \tag{5}$$

On the left hand side, the first two volume integrals are the acoustic stiffness and mass matrices, the third integral is related to the conditions at the boundary of the domain. The right hand side is composed of a volume and a surface source term.

The same operation on equation (4) gives the following weak form:

$$-\int_\Omega \nabla\phi\nabla p^{(1)} \, dV + k^2 \int_\Omega \phi p^{(1)} \, dV + \int_\Gamma \phi \partial_n p^{(1)} \, dS = -k^2 \int_\Omega \phi p^{(0)} \, dV. \tag{6}$$

The first difference between those formulations is that the unknown is not the same: in the former, one solves for the static pressure, while the acoustic component is studied in the latter. In order to compare them, the pseudo-sound shall be removed from the static pressure in equation (5).

The main distinction lays in the source term: both of them ($\underline{\underline{\nabla}} \cdot T_{ij}$ and $p^{(0)}$) can be computed with a CFD code, but the divergence of Lighthill's tensor is a vector of three components while the pseudo-sound is a scalar value. This implies that with equation (5), the size of the data exported from the CFD is thrice as much as the one with equation (6). Furthermore, while the pseudo-sound corresponds to one of the unknowns of an incompressible CFD solver, the divergence of Lighthill's tensor is not computed by default.

To compare these formulations, they have been implemented in a FEM solver and applied to a duct flow described in the following section.

3. APPLICATION TO A DUCTED FLOW

3.1 System description

The system on which we applied this study is a rectangular duct of 20 cm $\times$ 10 cm, equipped with a diaphragm. The mass flow inside the duct is around 0.17 m^3/s, resulting in a maximum Mach number of 0.15 and a Reynolds number of 45000. Consequently, the hypothesis of low Mach number and high Reynolds number might hold true.

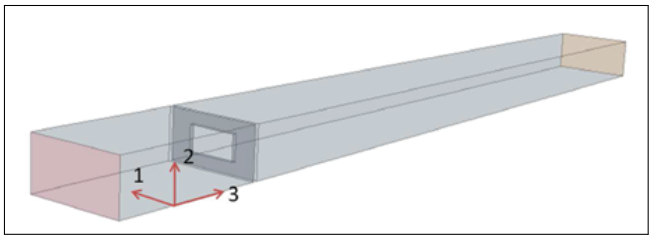

Figure 1. Computational domain.

This system has been extensively studied numerically at ESI [7, 8], as well as numerically and experimentally at the UTC, where the corresponding test bench has been set up. It is made up of a wind tunnel obstructed by a test section in which a diaphragm can be placed. Anechoic endings prevent wave reflections in the wind tunnel and at the outlet. This bench is equipped with a 2N-port system for the acoustic characterization of the test section. A PIV instrumentation can be installed to measure the aerodynamic features of the flow [9, 10]. The Figure 2 shows the test section corresponding to our diaphragm fitted in this wind tunnel.

Our numerical results will be compared with the experimental ones obtained by Bennouna [10].

3.2 Numerical setup and parameters

In order to solve the weak forms written above, the first step is to compute the source terms, respectively $\underline{\underline{\nabla}} \cdot T_{ij}$ and $p^{(0)}$ in the volume and their normal derivative at the

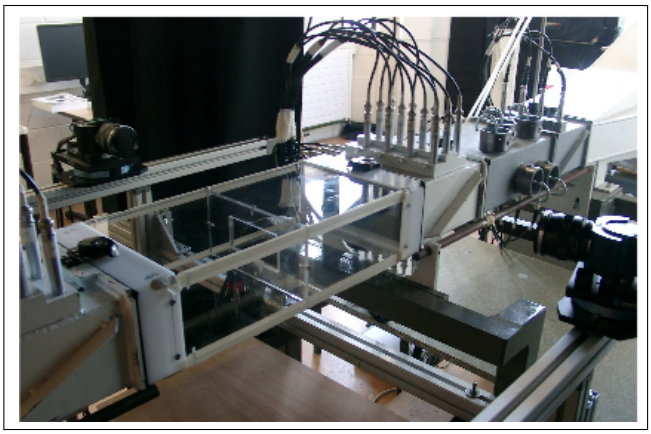

Figure 2. Test bench at the UTC.

boundaries. This is done by *Computational Fluid Dynamics* (CFD), through an unsteady simulation of the discretized weak equations on an unstructured grid. The chosen method is the *Large Eddy Simulation* (LES) with OpenFOAM [11], that solves the filtered incompressible Navier-Stokes equations, using a Smagorinsky sub-grid scale model. The inlet condition is based on the value of velocity obtained by PIV measurements, while the pressure is imposed at the outlet and a smooth wall condition is applied on the duct walls. During the computation, both source terms are computed and exported.

The meshes for CFD and FEM are not the same: in the CFD the smallest element size is driven by the smallest turbulent scale that has to be resolved according to the bandwidth targeted. The size of the elements should be smallest in the source region where strong gradients exist. Near the walls, thin prism layers are needed to resolve correctly the turbulent boundary layer. In the rest of the domain, the geometry of the elements can be arbitrary as long as some quality criteria are respected. In FEM, the size of the elements is fixed in such a way that approximately 10 linear elements or 5 quadratic ones fit in a wavelength for the highest frequency. Therefore, the CFD and FEM meshes are totally different: our CFD Mesh is composed of 10 millions of mostly tetrahedral cells generated with the software Centaur, while the FEM mesh is made of quadratic tetrahedron elements, resulting in 8000 nodes.

The amount of data exported from CFD is very large (three components of $\underline{\underline{\nabla}} \cdot T_{ij}$ and one scalar $p^{(0)}$ value per node, multiplied by the number of nodes in the mesh and the number of time steps). Therefore, those sources are interpolated on the nodes of the acoustic mesh on-the-fly with a conservative algorithm. In the present duct case, the volume of the data stored during the CFD on the FEM mesh is around tens of gigabytes. Without this key step, it would have been more than a terabyte for the same data on the CFD mesh.

As mentioned above, $\underline{\underline{\nabla}} \cdot T_{ij}$ cannot be directly exported from the CFD since this quantity is not computed by the solver. An on-the-fly post-processing step has been added in the simulation to compute it from the velocity field.

Once the source terms are obtained, they are transformed in the frequency domain. The time interval is split up into several segments. A FEM solver is then used to compute the acoustic propagation in the duct, a nodal solver working in the frequency domain. The duct walls are treated as rigid walls, and the boundary condition at the ends of the duct is a *Dirichlet to Neuman* (DtN) to ensure that the waves are not reflected, as in an infinite duct. It is assumed that the duct is long enough so that the turbulent field is damped before reaching the ends. The pressure fluctuations reaching the ends are therefore only acoustic ones. In this case, the normal derivative of the pressure can be written analytically using the duct modes and we have formally $\partial_n p = T(p)$. In equation (5), this relation is applied directly to the static pressure while in equation (6), it is applied to the acoustic part, and in this latter scenario, incompressible flow pressure fluctuations are neglected on both ends of the duct.

This DtN condition is also used to compute the acoustic power radiated in the duct:

$$\mathcal{P} = \frac{1}{2} Re \left\{ \frac{i}{\rho_0 \omega} \int_\Gamma p \cdot T^*(p) \, dS \right\}. \tag{7}$$

3.3 Results

The acoustic power levels computed with the two approaches are compared on the following figure. For both approaches, 15 time intervals have been used. The experimental curve comes from [12]. The cut-off frequencies of the modes are shown with vertical lines.

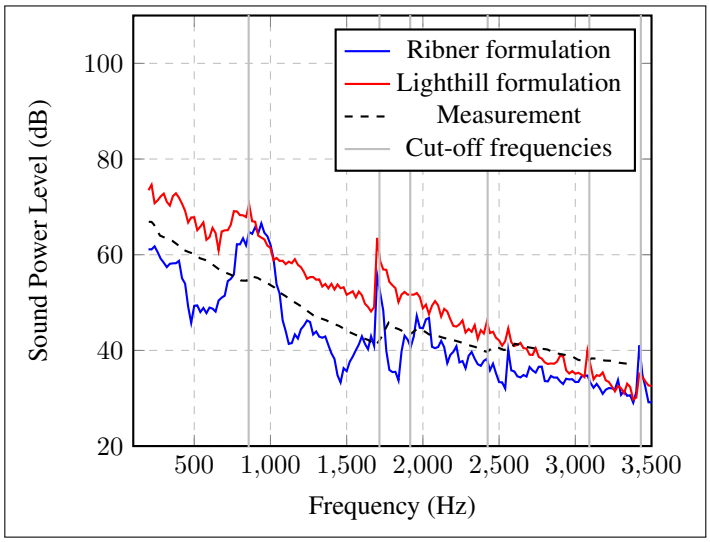

Figure 3. SWL computed with the different source terms.

First, one can observe that both numerical curve are in good agreement with the experimental one, and that Lighthill's analogy seems to be more accurate than Ribner's analogy in low frequency. The experimental results are smoother than the numerical ones since the number of time interval is more significant. As a matter of fact, increasing the number of segments with the numerical approach requires a longer CFD simulation and a larger volume of data to export and post-process before the FEM

computation. With the experimental approach, the cost is much less significant and increasing the duration of the measurement has a low impact on the duration of the post-processing.

While Lighthill's analogy seems to give better results, the associated source term $\underline{\underline{\nabla}} \cdot T_{ij}$ is more complex to obtain: firstly, this quantity is not a CFD variable and therefore not calculated by default. Its computation has to be added in the solver. Secondly, it is a vector quantity, which means that the volume of the data stored during the CFD is triple the one with Ribner's analogy. Solving Ribners's dilatation equation requires less data from the CFD, but even though the order of magnitude is correct, the radiated sound power level is slightly underestimated. Furthermore, the physical interpretation of the quantities manipulated is not trivial: while $p^{(1)}$ is considered as the "acoustic" component, it is not defined as such. It is more precisely the error committed by assuming the incompressibility of the flow, and thus contains the sound, the compressible fluctuation of the pressure. Some author prefer calling it the *corrective* pressure [13]. The physical quantity that must be studied is the sum of this corrective component and the pressure coming from the incompressible CFD.

To explain the differences between these results, a first comment is that in the Ribner approach, the DtN boundary condition is applied to the acoustic pressure and not the static one. Therefore, a surface term containing the normal derivative of the hydrodynamic pressure is neglected on both ends. Another important factor is that the order of derivation of the source terms are not the same: Ribners's source is directly a CFD quantity while Lighthill's one involves the divergence of a CFD field. This additional derivation may cause numerical errors.

The following figure shows the relative static pressure field on the duct walls and on a plane at half-height in the duct, at 1 kHz.

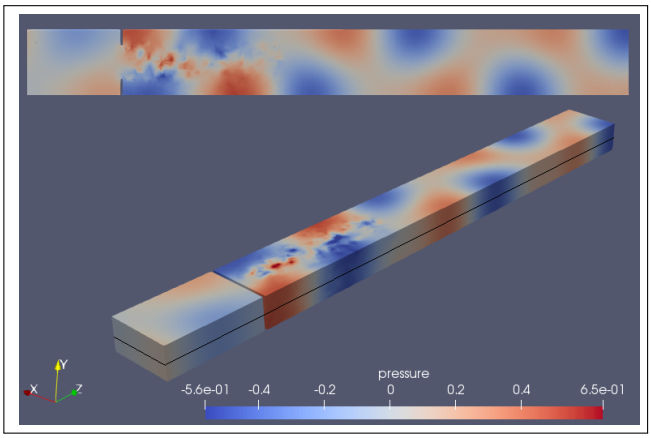

Figure 4. Hydrodynamic and acoustic pressure fluctuations.

One can clearly see the first non-planar mode propagating inside the duct, which cut-off frequency is around 860 Hz. Far from the diaphragm, the acoustic fluctuation is almost the only observable fluctuation. Right beyond the obstacle, the pressure field is more disordered, due to the turbulent pseudo sound resulting in this acoustic field.

4. CONCLUSION

Two different aeroacoustic approaches have been presented, combining FEM implementations of Lighthill and Ribner's analogies with the computation of the associated aerodynamic sources with CFD. The first step of the procedure is to compute the sound source with LES with the software OpenFOAM. During this step, the source information is mapped on a coarser acoustic mesh. Lastly the acoustic propagation is performed with a FEM solver working in the frequency domain.

This method has been applied to predict the sound generated by a ducted diaphragm and numerical results are compared with experimental ones.

Both numerical approaches are in a good agreement with the measurements. Lighthill's analogy seems to be slightly more accurate but is more complex to carry out for several reasons: first, the aerodynamic sound source is not directly accessible in the CFD simulation and an additional post-processing step has to be implemented. Then, the volume of the data exported during the CFD is more significant since the source term is a 3D vector, while Ribner's source is a scalar quantity. These hybrid approaches are a good compromise in terms of computational cost and accuracy, and therefore are applicable for industrial applications.

In the near future, these methods will be further extended in order to predict the noise generated by a fan inserted in a duct.

5. REFERENCES

[1] X. Gloerfelt, "Noise from automotive components," 01 2009.

[2] C. A. Wagner, T. Hüttl, and P. Sagaut, *Large-Eddy Simulation for Acoustics*. Cambridge Aerospace Series, Cambridge University Press, 2007.

[3] M. J. Lighthill, "On sound generated aerodynamically. i. general theory," in *Proc. of The Royal Society A: Mathematical, Physical and Engineering Sciences*, vol. 211, pp. 564–587, 03 1952.

[4] H. S. Ribner, *Aerodynamic sound from fluid dilatation: a theory of the sound from jets and other flows*. Toronto, Ontario: University of Toronto, Institute of Aerophysics, 1962.

[5] A. Oberai, F. Roknaldin, and T. Hughes, "Computational procedures for determining structural-acoustic response due to hydrodynamic sources," *Computer Methods in Applied Mechanics and Engineering*, vol. 190, pp. 345–361, 10 2000.

[6] S. Caro, P. Ploumhans, X. Gallez, R. Sandboge, F. Sahkib, and M. Matthes, "A new caa formulation based on lighthill's analogy applied to an idealized automotive hvac blower using acusolve and actran/la," in

11th AIAA/CEAS Aeroacoustics Conference, American Institute of Aeronautics and Astronautics, May 2005.

[7] N. Zerbib, L. Mebarek, and A. Heather, "Use of openfoam coupled with the finite element method for computational aeroacoustics," 2016.

[8] N. Zerbib, L. Mebarek, and A. Heather, "Wind noise application coupling openfoam with an aero- acoustic finite element hybrid method,"

[9] H. Trabelsi, *Banc d'essai et procédure pour la caractérisation des éléments d'un SCA par un système 2N-ports avec écoulement : validation et application à des sources aéroacoustiques*. PhD thesis, Université de Technologie de Compiègne, 2011.

[10] S. Bennouna, *Aeroacoustics characterization of elements and associations of automobile air ventilation systems*. PhD thesis, Université de Technologie de Compiègne, Sept. 2016.

[11] OpenCFD, *OpenFOAM v1912 manual: the open source CFD toolbox*, 2019.

[12] N. Papaxanthos, *Integral methods for the calculation of the air flow noise in ducts in the presence of fixed obstacles*. PhD thesis, Université de Technologie de Compiègne, Nov. 2016.

[13] N. Papaxanthos, E. Perrey-Debain, S. Bennouna, B. Ouedraogo, S. Moreau, and J.-M. Ville, "Pressure-based integral formulations of lighthill–curle's analogy for internal aeroacoustics at low mach numbers," *Journal of Sound and Vibration*, vol. 393, 01 2017.